Pergamon

Journal of Structural Geology, Vol. 18, No. 6, pp. 835 to 845, 1996

0191-8141/96 $15.00 + 0.00

0191-8141(95)00139-5

Variation in fault-slip directions along active and segmented normal fault systems

GERALD P. ROBERTS

The Research School of Geological & Geophysical Sciences, Birkbeck College & University College London, Gower Street, London WC1E 6BT, U.K.

(*Received* 13 *March* 1995; *accepted in revised form* 22 *November* 1995)

Abstract—Local fault-slip directions show a systematic variation over distances of 20–35 km along the active and segmented Gulf of Corinth normal fault system, central Greece. Where fault throws are large (several km) close to the centres of fault segment map traces, local fault-slip directions parallel the regional N–S (±20°) slip-vector azimuth interpreted from earthquake focal mechanisms. However, where fault throws are small (tens of metres) close to fault segment boundaries, local fault-slip directions are oriented ~NE–SW when measured close to the western ends of fault segments, and ~NW–SE close to the eastern ends of fault segments. Local fault-slip directions change by ~90° across fault segment boundaries. It is suggested that fault-slip directions close to fault segment boundaries record local strain patterns at fault tips so that care should be taken when using this information during attempts to infer regional stress trajectories. Copyright © 1996 Elsevier Science Ltd

INTRODUCTION

Central Greece is undergoing crustal extension above the Hellenic Subduction Zone and at the western end of the North Anatolian Fault (Jackson 1994 and references therein). Focal mechanisms for normal faulting earthquakes in this region suggest that the regional slip-vector azimuth across the segmented normal fault system in the Gulf of Corinth is N–S (±20°), and this is confirmed by limited studies of lineations on faults (Roberts & Jackson 1991). However, it has been suggested recently that because hangingwall subsidence exceeds footwall uplift during normal faulting, greater along-strike extension occurs in the hangingwall than in the footwall along segmented normal fault systems (Wu & Bruhn 1994, Ma & Kusznir 1995). This asymmetry in along-strike extension is thought to induce oblique fault-slip close to fault segment boundaries where low fault displacements occur; along a normal fault dipping north, right-lateral oblique fault-slip should occur at the western termination of the fault, whilst left-lateral oblique fault-slip should occur at the eastern termination of the fault.

The purpose of this study is to assess whether this pattern of kinematics can be seen in the field along segmented normal faults, and hence whether local fault-slip directions recorded by lineations on faults (Figs. 1, 2 and 3), are (1) a record of how the orientation of the principal axes of finite strain vary along segmented normal faults, or (2) local records of stress orientations which can be combined to infer regional stress trajectories (Angelier 1979, 1984, Mercier *et al.* 1979, Angelier *et al.* 1982a,b, Pavlides & Mountrakis 1987).

The first part of the paper describes how the Gulf of Corinth Fault System can be divided into fault segments using data concerned with displacement gradients and spatial variations in Pliocene–Recent slip rates. The second part of the paper describes how the kinematics of faulting vary along the strike of the fault segments defined in the first part of the paper. The result of this description of fault kinematics is that local fault slip-directions vary in a systematic and predictable manner in accordance with variations in fault displacement. The implications of these findings are then discussed.

SEGMENTATION OF THE GULF OF CORINTH FAULT SYSTEM

A preliminary division of the Gulf of Corinth Fault System into fault segments can be made by examining displacement gradients evident on published geological maps (Poulimenos *et al.* 1989, Piper *et al.* 1990, Doutsos & Poulimenos 1992, Poulimenos 1993, IGME 1970, 1971, 1982, 1984a–c, 1985, 1989a, 1993) and offshore seismic, well and side-scan sonar data (Heezen *et al.* 1966, Myrianthis 1982, Perissoratis *et al.* 1986, Ferentinos *et al.* 1988, Higgs 1988, Roberts & Gawthorpe 1995) (Fig. 2). In particular, fault displacement gradients can be recognised by examining along-strike variations in footwall topography and the elevation of the rocks forming the pre-rift stratigraphy. For example, Fig. 2 shows that the highest elevations of pre-rift stratigraphy vary systematically along the strike of the fault system, as does the footwall topography (Fig. 4). The highest pre-rift elevations and the highest topography are located in the footwalls of the interpreted fault segments close to the centres of their map traces, with values decreasing towards their lateral terminations. In this study, footwall topography is used to infer fault displacements as is common practice in studies of extensional fault systems (Crone & Haller 1991, Gawthorpe & Hurst 1993); thus, the areas of low topography indicate low fault displacement and these areas are suggested to be fault segment boundaries. Note that examination of (1)

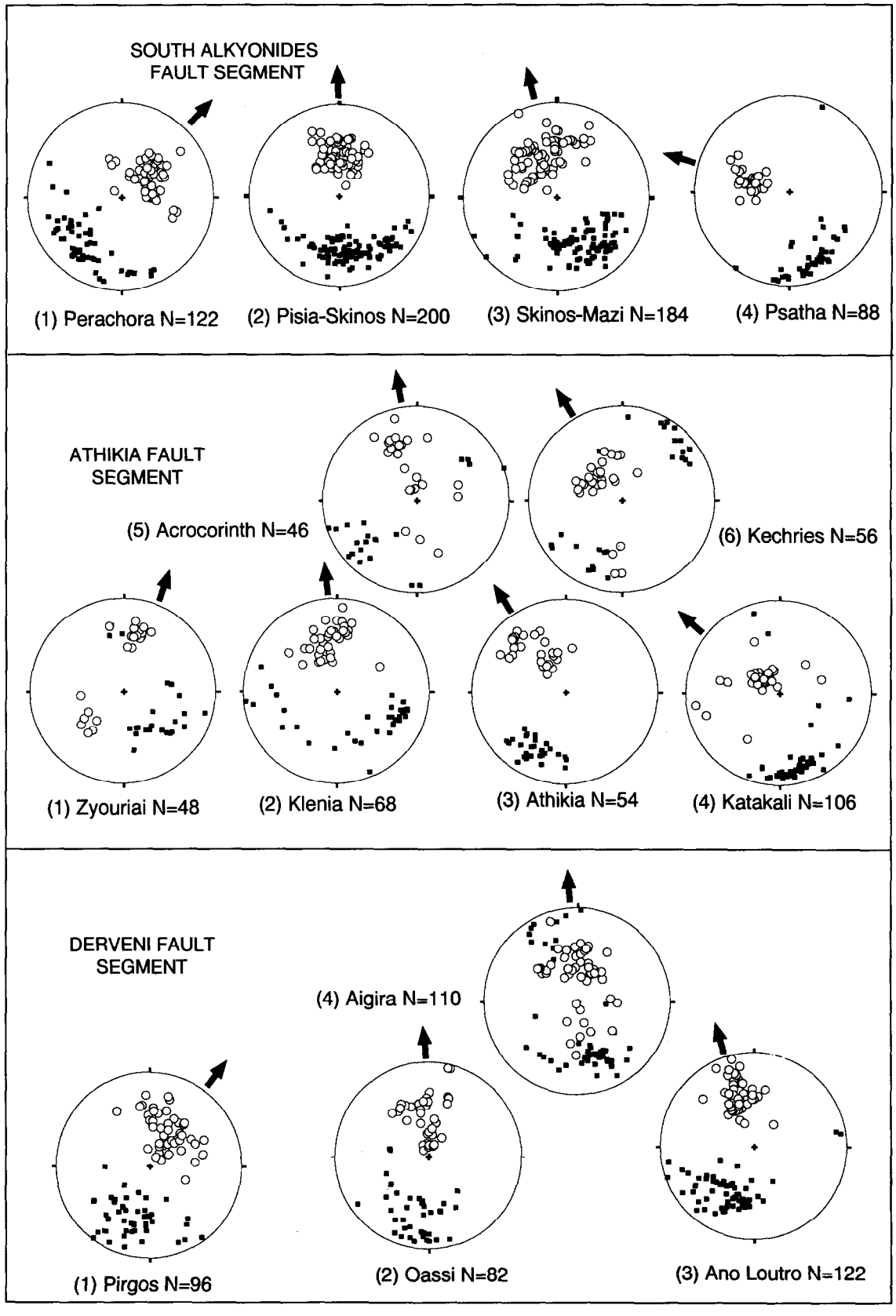

Fig. 1. Lower hemisphere stereographic projections of poles to fault planes (filled squares) and lineations on fault planes (open circles) for the Gulf of Corinth. The 30 localities are named after the closest town or village and the locality numbers are shown on Fig. 2. Measurements were made of all faults and lineations that intersected traverse lines across exposures. Measurements were taken from the faulted contacts between the pre-rift and syn-rift rocks, and from fault planes located in the footwall of these contacts. In the case of the South Alkyonides Segment, measurements for Locality 2 were taken from 15 exposures $<400\ m^2$ in area within an area of $\sim 60\ km^2$ (see Fig. 3) and from 5 exposures $<400\ m^2$ in area within an area of $\sim 20\ km^2$ for Locality 4. In all other examples the measurements were taken from single exposures $<400\ m^2$ in area. Arrows appended to the stereonets give a visual guide to the fault slip direction interpreted from the stereonet, and these arrows have been transferred onto Fig. 2.

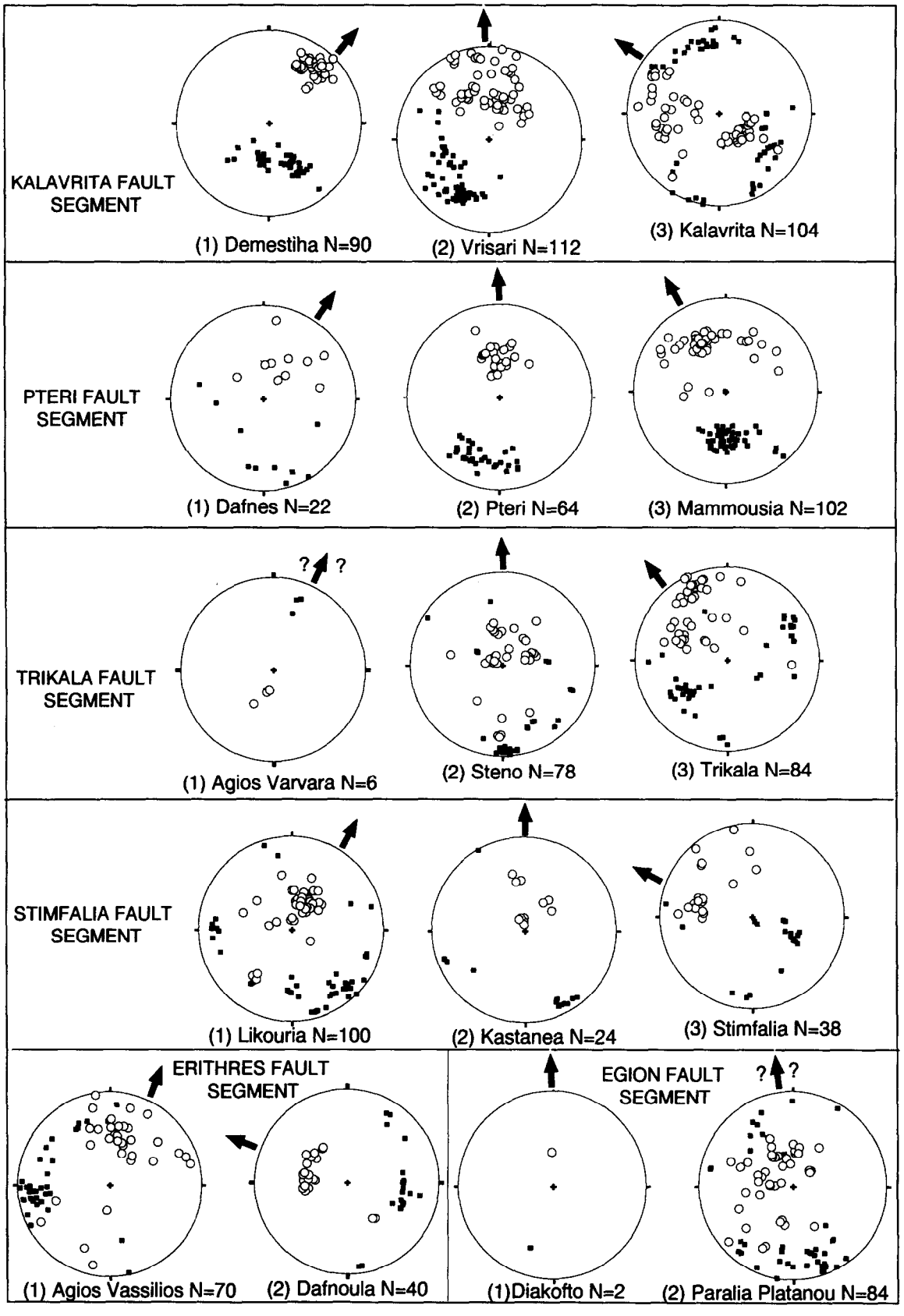

Fig. 1. *Continued.*

hangingwall topography and (2) the elevation of the pre-rift in the hangingwall, confirms this interpretation of the positions of fault segment boundaries. The lowest hangingwall topography/bathymetry and the lowest elevations of the pre-rift stratigraphy are found in the hangingwalls of the fault segments close to the centres of their map traces, with values increasing towards the proposed fault segment boundaries (Figs. 2 and 5a & b). These variations in topography and elevation of the pre-rift stratigraphy show that fault displacements vary from several kilometres in the central portions of the fault segments, to tens of metres or less close to fault segment boundaries. The fault segments resemble the isolated segments that are thought to exist early during the evolution of normal fault systems (Anders & Schlische 1994).

Following examination of published accounts of the thicknesses and internal geometries of the syn-rift deposits, it becomes clear that fault-slip rates vary in tandem with fault displacements. For example, seismic lines located around the offshore portions of the fault system (XFS and the central part of the SAFS) show that the greatest thicknesses of syn-rift deposits exist in the hangingwall close to the centres of the segment map traces, decreasing towards the fault segment boundaries proposed in this study (Myrianthis 1982, Higgs 1988) (Figs. 2 and 5a & b). This indicates that the highest subsidence rates and hence the highest fault-slip rates exist close to the centres of the map traces of the proposed segments. In addition, fan/delta deposits display clinoforms several hundred metres in height and aggradational sequence geometries close to the centres of segment map traces (Dart *et al.* 1994), with sheet-like sequence geometries close to fault segment boundaries (Figs. 2 and 5c & d). These variations in the internal geometry of syn-rift deposits also show that the highest subsidence rates and fault-slip rates must exist close to the centres of segments in order to produce the significant fault-controlled palaeotopography necessary for the development of large clinoforms. Subsidence and uplift rates together with fault-slip rates must decrease towards the fault segment boundaries in order to produce the sheet-like sediment sequence geometries and relatively thin hangingwall sediment thicknesses that exist in these localities.

In summary, it appears that the structure of the Gulf of Corinth Fault System in the area studied is dominated by the existence of ten fault segments that are ~20–35 km in length.

THE GEOMETRY AND KINEMATICS OF FAULT SEGMENTS AROUND THE GULF OF CORINTH

The kinematics of the fault segments described earlier were investigated by measuring 1201 lineations on fault planes from 30 localities (Fig. 1) lying either close to the proposed fault segment boundaries, or the centres of fault segment map traces; the orientations of the fault planes were also recorded and are shown as poles to fault planes in Fig. 1. All the lineations were measured from fault planes developed in pre-rift Mesozoic rocks; some were measured from the main faulted contacts between pre-rift rocks and syn-rift rocks whilst others were measured from minor faults within the footwalls of such contacts.

Let us first examine the orientations of fault planes. At the scale used in Fig. 2 it is not possible to show all the faults that are present; faults dipping to the ~south, ~east and ~west exist, but are not shown on this map because, generally, they have relatively small throws (a few tens of metres) (for examples see Poulimenos *et al.* 1989, Piper *et al.* 1990, Doutsos & Poulimenos 1992). However, note that faults dipping ~south, ~east and ~west are represented in the scatter in poles to fault planes shown in Fig. 1. Scatter in fault plane orientations also reflects the existence of smaller-scale features than the ~south-, ~east- and ~west-dipping faults; lateral and oblique ramps exist within small-scale transfer zones (Fig. 3) and on an even smaller scale, corrugations occur on single fault planes. The effect of variation in fault plane orientations on fault-slip directions will be discussed later.

Scatter also exists in the fault-slip directions indicated by lineations on fault planes (Fig. 1). However, note that despite this scatter, clusters of lineations measured from

Fig. 2. (a) Map showing the geology, topography and bathymetry of the area around the Gulf of Corinth. (b) Interpretation of (a) showing the positions of fault segments, fault segment boundaries and historical earthquakes (<Ms 5.8) for the last ~100 years around the Gulf of Corinth. CB, Corinth Basin; GA, Gulf of Alkyonides; MB, Megara Basin; ETB, Erithres/Thiva Basin; DB, Derveni Basin; PB, Pteri Basin; KB, Kalavrita Basin; TB, Trikala Basin; SB, Stimfalia Basin; M, Mediterranean; P, Peloponnese; IC, Isthmus of Corinth; HSZ, Hellenic Subduction Zone; NAF, North Anatolian Fault; KFS, Kalavrita Fault Segment; PFS, Pteri Fault Segment; EgFS, Egion Fault Segment; DFS, Derveni Fault Segment; TFS, Trikala Fault Segment; SFS, Stimfalia Fault Segment; XFS, Xilokastro Fault Segment; AFS, Athikia Fault Segment; SAFS, South Alkyonides Fault Segment; EFS, Erithres Fault Segment. The zones of NNW- and NNE-striking faults have been adapted from Poulimenos *et al.* (1989) and from the author's own field observations. Fault displacements can be assessed qualitatively by examining the differences in spot heights across faults. Spot heights located on pre-rift indicate the minimum elevation of the top of the pre-rift and spot heights on syn-rift are close to the maximum elevations for the top of the pre-rift. Variations in fault throw are revealed by (1) the increase in the minimum elevation of the top of the pre-rift in the footwalls towards the centres of some segments (e.g. DFS, AFS, SAFS & EFS) (see also Fig. 4), and (2) the decrease in the maximum elevation of the pre-rift in the hangingwalls towards the centres of other segments (e.g. SAFS & EFS). Where faults have pre-rift in both the hangingwall and footwall this generally indicates that fault displacements are small (except the TFS where uplift, erosion and river incision have removed the syn-rift suggesting that the fault segment continues further west). Long term (10^5–10^6 yrs) fault slip rates can be estimated from the geometries of syn-rift sediments and from isopach maps interpreted from seismic sections. High slip rates away from the tips of segment map traces have allowed the accumulation of relatively thick syn-rift (Myrianthis 1982, Perissoratis *et al.* 1986, Higgs 1988). Where fault slip-rates are high relative to infilling of fault-related topography by sedimentation, fan/deltas with large (~300 m high) clinoforms have formed (Dart *et al.* 1994). Local N–S fault-slip directions on the EgFS and offshore geophysical data (Heezen *et al.* 1966, Higgs 1988, Ferentinos *et al.* 1988) suggest that the segment continues offshore.

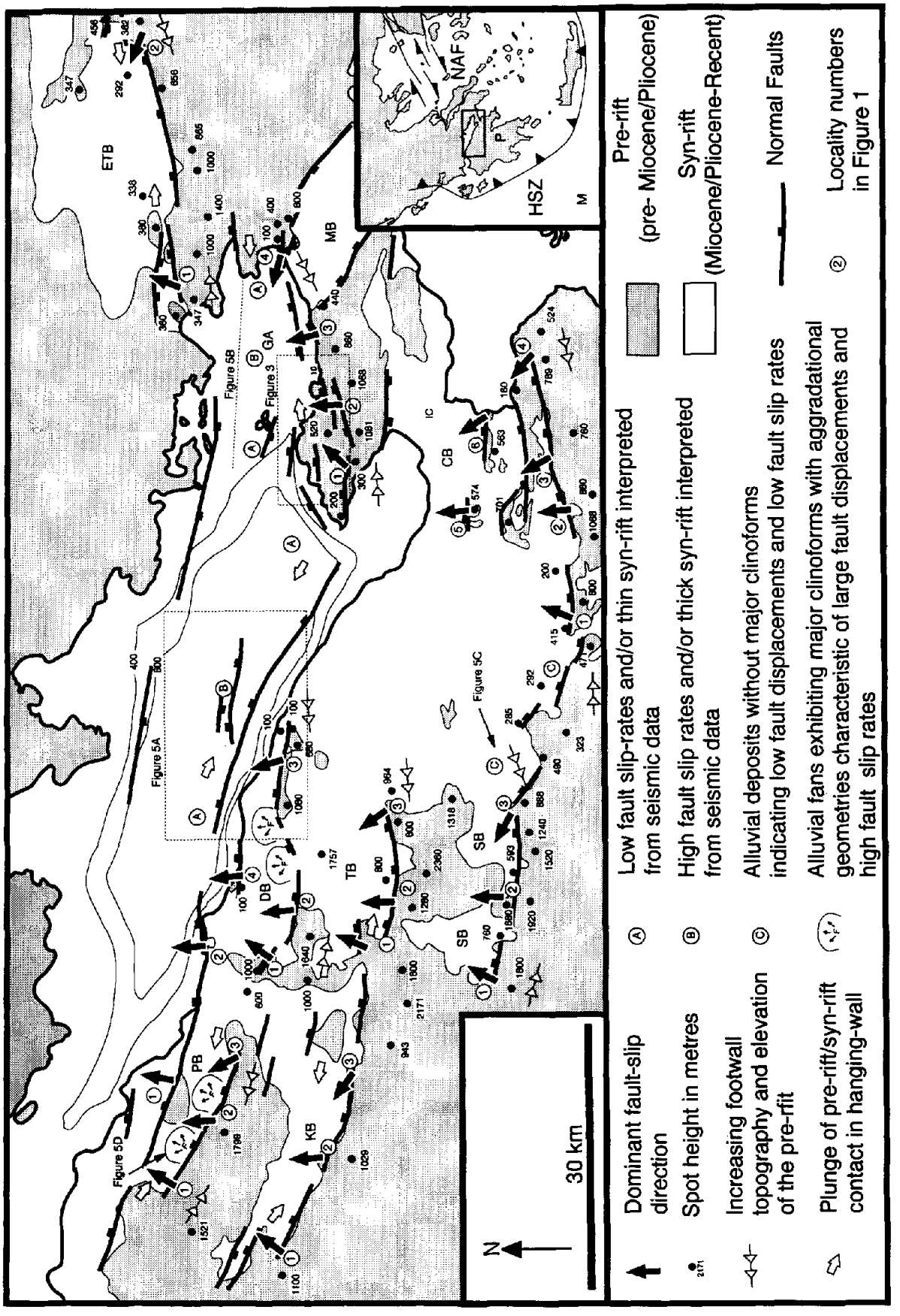
ETB
MB
GA
IC
CB
SB
TB
DB
PB
KB
Figure 5A
Figure 5B
Figure 3
Figure 5C
Figure 5D
NAF
HSZ
N
30 km
Dominant fault-slip direction
Spot height in metres
Increasing footwall topography and elevation of the pre-rift
Plunge of pre-rift/syn-rift contact in hanging-wall
Low fault slip-rates and/or thin syn-rift interpreted from seismic data
High fault slip rates and/or thick syn-rift interpreted from seismic data
Alluvial deposits without major clinoforms indicating low fault displacements and low fault slip rates
Alluvial fans exhibiting major clinoforms with aggradational geometries characteristic of large fault displacements and high fault slip rates
Pre-rift (pre- Miocene/Pliocene)
Syn-rift (Miocene/Pliocene-Recent)
Normal Faults
Locality numbers in Figure 1

Fig. 2a.

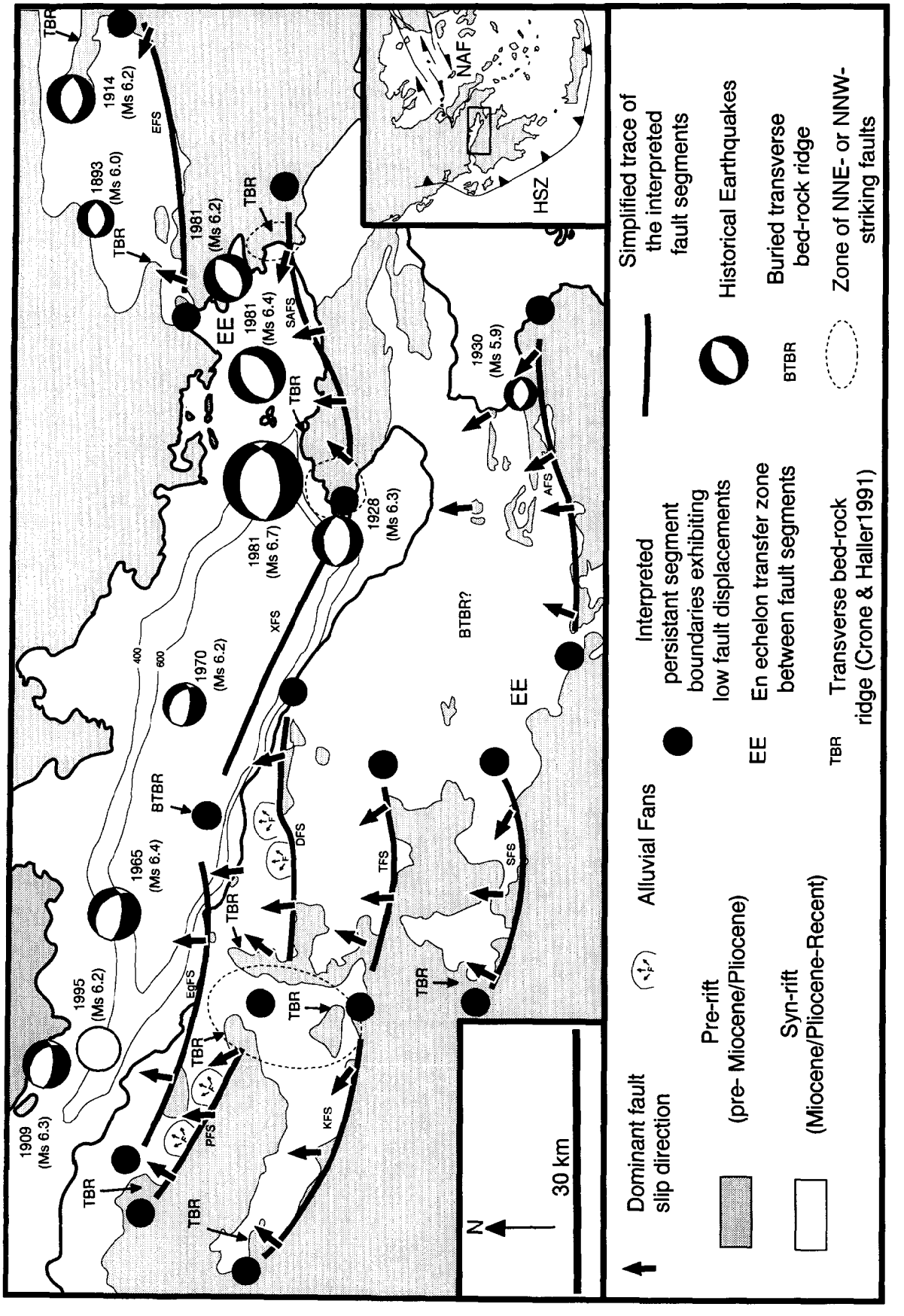
1909 (Ms 6.3)
1995 (Ms 6.2)
1965 (Ms 6.4)
1970 (Ms 6.2)
1981 (Ms 6.7)
1928 (Ms 6.3)
1981 (Ms 6.4)
1981 (Ms 6.2)
1893 (Ms 6.0)
1914 (Ms 6.2)
1930 (Ms 5.9)
TBR
BTBR
BTBR?
EE
EFS
PFS
KFS
DFS
TFS
SFS
XFS
SAFS
AFS
400
600
NAF
HSZ
N
30 km
Dominant fault slip direction
Alluvial Fans
Interpreted persistant segment boundaries exhibiting low fault displacements
Simplified trace of the interpreted fault segments
Historical Earthquakes
Pre-rift (pre- Miocene/Pliocene)
Syn-rift (Miocene/Pliocene-Recent)
En echelon transfer zone between fault segments
Buried transverse bed-rock ridge
Transverse bed-rock ridge (Crone & Haller1991)
Zone of NNE- or NNW-striking faults

Fig. 2b.

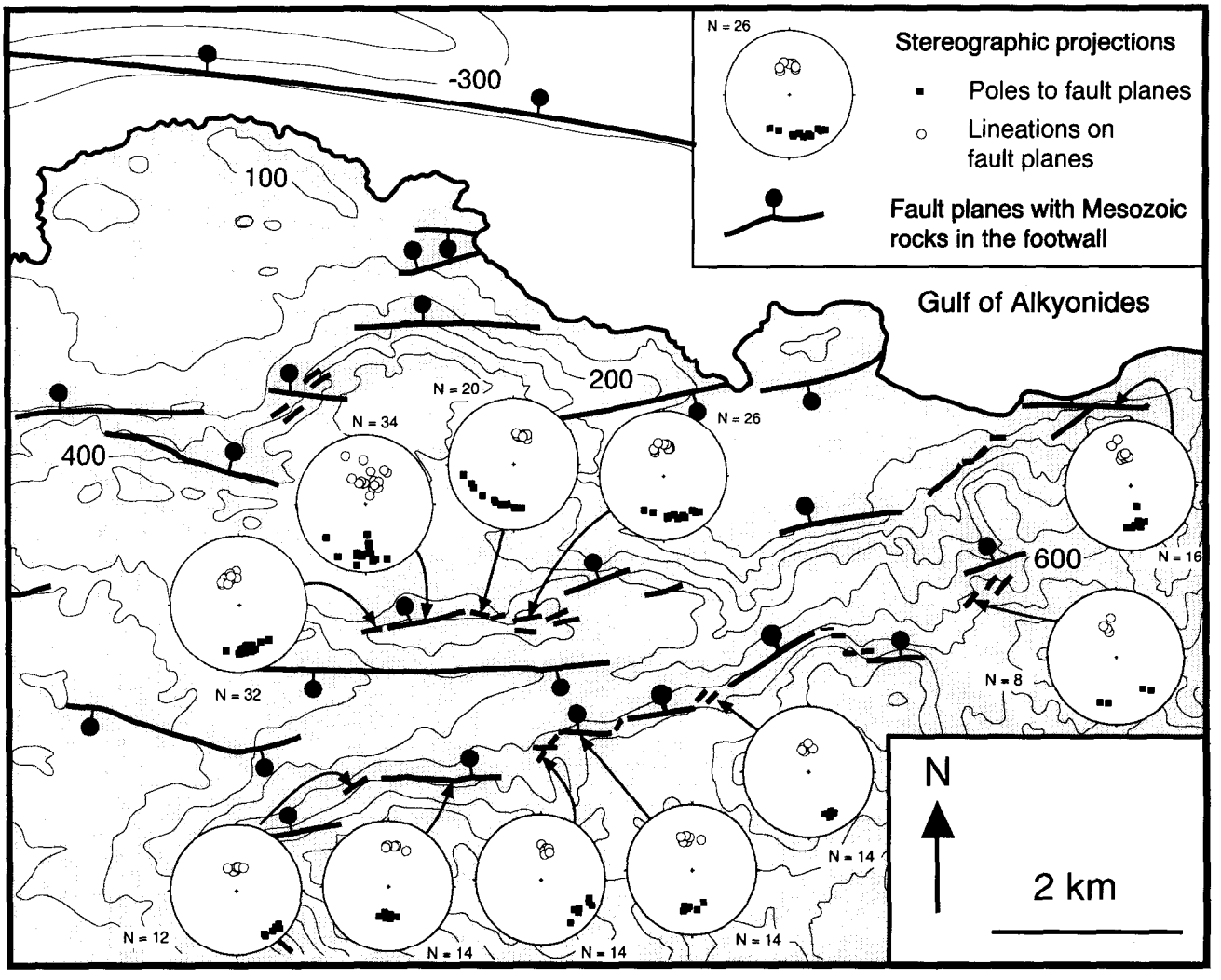

Fig. 3. Map showing the geometrical complexity along the South Alkyonides Fault Segment (see Figs. 1 and 2). Small faults (~1–3 km in length) are offset across small transfer zones (<2 km^2). Lower hemisphere stereographic projections for 11 exposures (<400 m^2 in area) are presented with the orientations of poles to fault planes (filled squares) and lineations on fault planes (open circles) plotted. Implied fault-slip directions are ~N–S regardless of whether the exposure lies along a fault ~1–3 km in length or within a transfer zone containing minor faults <300 metres in length. Thus, changes in fault orientation along the fault segment do not produce local fault-slip directions that deviate from regional slip-vector azimuths.

opposite ends of the same fault segment do not overlap on the stereographic projections (e.g. compare the clusters of lineations measured from localities (1) and (4) from the South Alkyonides Fault Segment or (1) and (3) from the Kalavrita Fault Segment). The author interprets this to indicate that the dominant fault-slip direction changes along the fault segments. Interpreted dominant fault-slip directions are indicated on Fig. 1 as arrows fitted by eye through the data. Note that, despite the fact that measurements were made of all lineations that intersected traverse lines across exposures, the mean values for fault-slip directions have not been calculated. This is because the author feels that (1) the number of measurements is too small at some localities, and (2) the faults are not completely exposed so that the data may be skewed towards orientations of lineations that are best exposed.

Nevertheless, if the proposed dominant fault-slip directions are accepted, note that close to the centres of the map traces of the fault segments, lineations indicate ~N–S fault-slip (Figs. 1, 2 and 3). This is in good agreement with the N–S (±20°) regional slip-vector azimuth across the Gulf of Corinth Fault System interpreted from earthquake focal mechanisms (Roberts & Jackson 1991, Jackson 1994). In contrast, close to the western ends of fault segments, ~NE–SW fault-slip predominates with ~NW–SE fault-slip close to the eastern fault segment boundaries. Thus, it appears that fault-slip directions vary as a function of fault displacement, with fault-slip directions changing by ~90° across fault segment boundaries (Fig. 4). These observations indicate, in general, right-lateral oblique fault-slip at the western terminations of the fault segments and left-lateral oblique fault-slip at the eastern terminations of the fault segments in accordance with theoretical strain patterns proposed for normal faults (Wu & Bruhn 1994, Ma & Kusznir 1995) (see earlier).

It was stated earlier that the map of fault traces is rather simplified (Fig. 2a), because at the scale used, it is difficult to show more detail. However, in a more detailed map view (Fig. 3), small-scale structural complexity is evident, due to the presence of small transfer

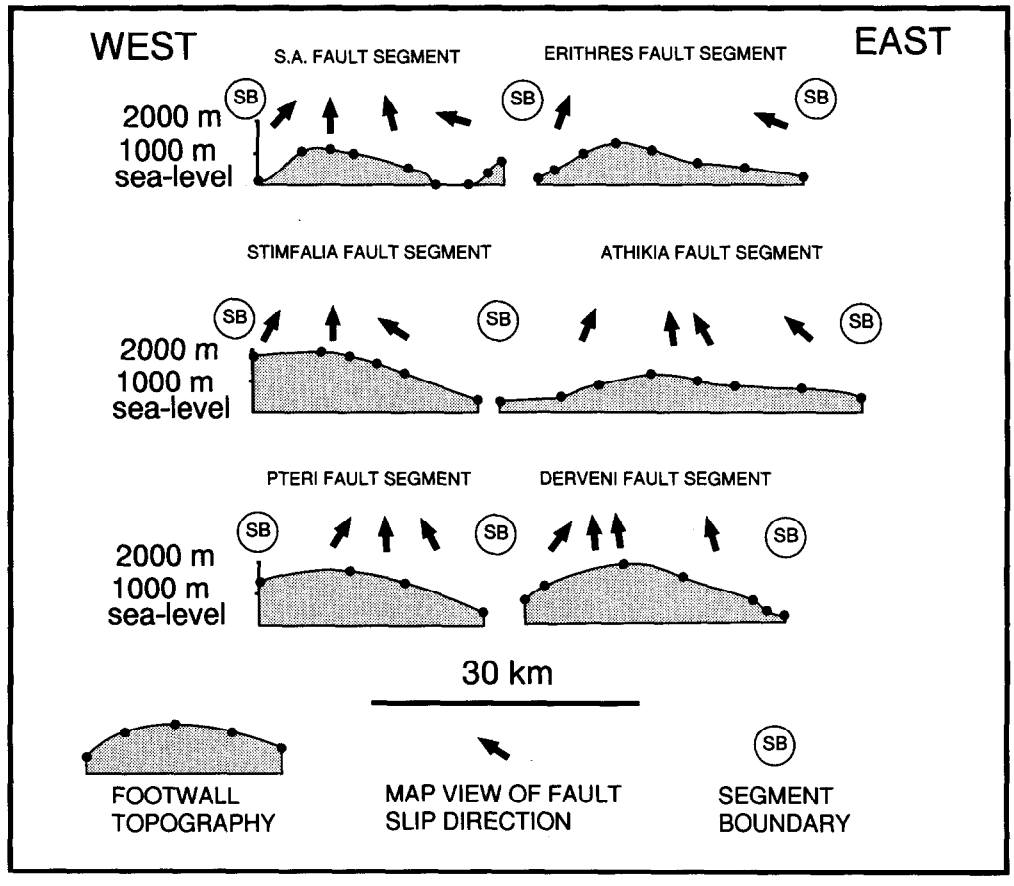

Fig. 4. Topographic profiles along the footwalls of fault segments in the Gulf of Corinth with local fault-slip directions superimposed. The topographic profiles have been constructed using spot heights from published maps (IGME 1970, 1971, 1982, 1984a,b, 1985, 1989a,b, 1993) to show the highest topography present, without the detail of minor valleys. The increase in footwall topography signifies an increase in fault displacements. Note that maximum footwall topography increases away from fault segment boundaries characterised by fault-slip directions (taken from Fig. 1) that are oblique to the regional N–S slip-vector azimuth. Also note that local fault-slip directions change by ~90° across fault segment boundaries.

zones (<2 km across) containing ~ENE and ~WNW trending faults, and this is an ubiquitous feature of the other segment map traces in Fig. 2 (e.g. see Poulimenos *et al.* 1989, Doutsos & Poulimenos 1992, Poulimenos 1993, Dart *et al.* 1994, Roberts & Gawthorpe 1995). Note, however, that the N–S fault-slip direction is evident across the area shown in Fig. 3, despite complexities in the fault geometry produced by small-scale transfer zones. Thus, it appears that the fault-slip directions are not controlled by the orientation of the faults that host the lineations; these small-scale transfer zones do not divide the fault system up into separate kinematic units with different fault-slip directions in the manner of the larger transfer zones and gaps in the fault system (~10–15 km across) shown in Fig. 2. As a result, it is suggested here that because fault throws, slip rates and fault kinematics vary systematically over distances of 20–35 km, the Gulf of Corinth Fault System should be sub-divided into ten segments that are 20–35 km in length rather than into smaller units defined by small-scale transfer zones (compare with Doutsos & Poulimenos 1992) (Figs. 2 and 4). The intervening fault segment boundaries appear to be ~10–15 km across, a dimension which is in good agreement with the dimensions of fault segment boundaries measured in other active extensional basins (e.g. Zhang *et al.* 1991).

An interesting point is that NNE- and NNW-trending faults exist within some of the fault segment boundaries around the Gulf of Corinth (Figs. 1 and 2b) (IGME 1984c, Poulimenos *et al.* 1989, Poulimenos 1993, Roberts unpubl. data); they are not shown as single fault surfaces on Fig. 2 because they have relatively small throws compared to the ~E–W faults. Where examined, these faults, which strike at high angles to the main ~E–W faults, are dip-slip faults accommodating extension along the strike of the fault system (e.g. see fig. 8B of Poulimenos *et al.* 1989, and Localities (1) and (4) of the SAFS in Fig. 1). These faults, therefore, resemble *release faults* (*sensu* Destro 1995) rather than *transfer faults* (*sensu* Gawthorpe & Hurst 1993) which transfer displacement between offset normal faults by strike-slip motions. It may be that these NNE–NNW dip-slip faults form to accommodate along-strike extension in positions where these motions cannot be accommodated by oblique-slip on the ~E–W faults, that is where displacements on the ~E–W faults decrease within the proposed fault segment boundaries.

In conclusion, the author suggests that the ~NE–SW

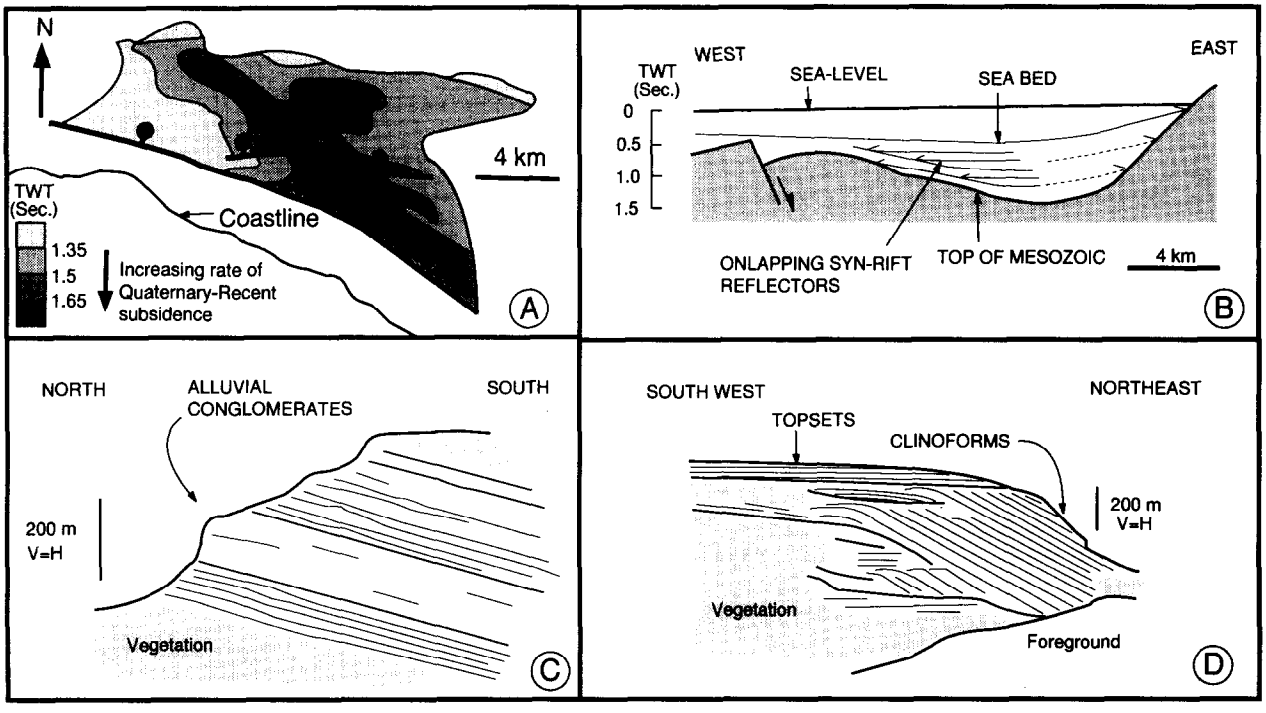

Fig. 5. Variation in the thicknesses and internal geometries of syn-rift deposits around the Gulf of Corinth. (a) Isochron map for the interval between a Quaternary syn-rift reflector and the sea-bed, re-drawn from Higgs (1988). Increase in two-way travel-time signifies an increase in sediment thickness. The variations in sediment thickness result from variations in subsidence and fault-slip rates from minima in the WNW and ESE, to a maxima between these two areas. (b) Line drawing of a seismic reflection profile (adapted from Myrianthis 1982) with additional information added to the eastern end of the cross-section taken from the author's own field observations and outcrop data (IGME 1984a). Prominent syn-rift reflectors (? Pliocene–Recent) onlap Mesozoic basement in the west of the cross-section (Myrianthis 1982) and Pliocene-recent deposits onlap Mesozoic limestones at the eastern end of the cross-section. The rates and magnitudes of subsidence, and presumably the slip rates on the basin-bounding fault system to the south (SAFS), increase from minima in the east and west to a maxima south of around the centre of the cross-section. (c) Line drawing of incised gorge sections through alluvial conglomerates from author's own field observations near to the fault segment boundary east of Stimfalia. The lack of large clinoforms and aggradational to progradational sequence geometries result from the low palaeo-structural relief and the low fault-slip rates which characterise this area. (d) Line drawing of incised gorge sections through the Keranitis Fan/Delta adapted from Gawthorpe *et al.* (1984), and from the author's own field observations. This fan/delta lies close to the centre of the map trace of the Pteri Fault Segment. The large clinoforms and aggradational to progradational sequence geometries result from the palaeo-structural relief and high slip-rates relative to infilling by sediment reported for this location (Dart *et al.* 1994, Gawthorpe *et al.* 1994).

and ~NW–SE fault-slip directions associated with oblique-slip faulting recorded around the Gulf of Corinth are produced because footwall uplift is greater than hangingwall subsidence along normal faults. Where fault displacements decrease close to fault segment boundaries, the asymmetry between along-strike extensional strains in the footwall and hangingwall induces (1) oblique-slip faulting in these localities as envisaged by Wu & Bruhn (1994) and Ma & Kusznir (1995), and (2) dip-slip normal faults in fault segment boundaries accommodating along-strike extension.

DISCUSSION AND CONCLUSIONS

It appears that local fault-slip directions only reflect the regional slip-vector azimuth across the Gulf of Corinth implied by earthquake focal mechanisms if they are measured from the centres of the map traces of fault segments. This is due to spatial variation in the strain patterns along the segmented normal faults in this area. It is suggested, therefore, that care should be taken not to include lineation data from localities close to fault segment boundaries when attempting to produce maps of regional stress trajectories, because the strain patterns in these localities are not well understood; more work is needed. However, if knowledge of strain patterns around segmented normal faults is incorporated into studies, it may then be possible to interpret both the regional stress trajectories *and* local complications of this stress field induced by fault segmentation using the classic techniques for study of fault-slip data (Angelier 1984 and references therein). Knowledge of local complications in strain and stress patterns at the lateral tips of normal faults will provide important insights into how the discontinuous faulting of the upper crust in central Greece, which involves extension and clockwise rotation about vertical axes, can be reconciled with the continuous flow patterns envisaged for the underlying lithosphere in this region (Taymaz *et al.* 1991, Jackson 1994).

An interesting consequence of this study is that because local fault-slip directions vary by ~90° across fault segment boundaries, we now have a new way of con-

straining the positions and dimensions of fault segments. By recognising areas where ~90° changes in fault-slip direction occur, we can pin-point areas that have persistently been starved of fault displacement and this information can be used in disciplines outside that of structural geology. Two examples of this are discussed below.

(1) Knowledge of the positions along normal fault systems where low fault displacements exist can be used in seismic hazard analysis, because such areas may represent places where the majority of past earthquake ruptures have terminated. If (a) a Characteristic Earthquake Model is adopted, and (b) maximum expectable earthquake magnitudes are considered to be a function of the dimensions of fault segments (Slemmons 1977, Hanks & Kanamori 1979, Wyss 1979, Bonilla *et al.* 1984, Schwartz 1989, Abercrombie & Leary 1993), we can use spatial variation in fault kinematics alongside other indicators of segment dimensions (see Crone & Haller 1991) to help assess the maximum expectable magnitudes of future earthquakes and hence seismic hazards in a region. This is discussed further by Roberts & Koukouvelas (in press).

(2) Gawthorpe *et al.* (1994) suggest that because uplift/subsidence vary spatially in a predictable manner along segmented normal faults, it should be possible to predict spatial variations in the drainage patterns, sedimentary facies and stratigraphic geometries of syn-rift deposits for marine-influenced basins if we have knowledge of (a) the positions and dimensions of fault segments, (b) eustatic sea-level curves and (c) the volumes of sediment entering depositional environments. The result of the study presented in this paper is that for the first time, the positions and dimensions of fault segments around the Gulf of Corinth are known. Thus, in the future, studies of the development of the syn-rift deposits around the Gulf of Corinth can be carried out within a framework of fault segmentation. Study of fault-slip directions in other extensional basins may provide similar constraints.

In conclusion, spatial variations in fault kinematics can be used as a tool to assess fault segmentation, a feature which appears to be ubiquitous within all of the earth's rifts.

Acknowledgements—This study was funded by NERC GR9/1034 and Birkbeck College. IGME is thanked for permission to conduct field studies. I thank Iain Stewart, Ann-Marie Scott, Robin Pilcher, David Scott, Brin Roberts, Andy Samuels, Gianluca Valensise, James Jackson, John Platt, Athanassios Ganas, Ioannis Koukouvelas and Theodor Doutsos for discussions concerning the kinematics of active faults in Greece. Mike Beling is thanked for pointing out the existence of NNW-striking faults at the western termination of the SAFS. I also thank Eric Barrier, Richard Lisle and an anonymous referee for their comments.

REFERENCES

Abercrombie, R. & Leary, P. 1993. Source parameters of small earthquakes at 2.5 km depth, Cajon Pass, southern California: implications for earthquake scaling. *Geophys. Res. Lett.* **20**, 1511–1514.

Anders, M. H. & Schlische, R. W. 1994. Overlapping faults, intrabasin highs and the growth of normal faults. *J. Geol.* **102**, 165–180.

Angelier, J. 1979. Determination of the mean principal directions of stresses for a given fault population. *Tectonophysics* **56**, T17–T26.

Angelier, J. 1984. Tectonic analysis of fault slip data sets. *J. Geophys Res.* **89**, 5835–5848.

Angelier, J., Lyberis, N., Le Pichon, X., Barrier, E. & Huchon, P. 1982a. The tectonic development of the Hellenic Arc and the Sea of Crete. *Tectonophysics* **86**, 159–196.

Angelier, J., Tarantola, A., Valette B. & Manoussis, S. 1982b. Inversion of field data in fault tectonics to obtain the regional stress—1. Single phase fault populations: A new method of computing the stress tensor. *Geophys. J. R. Astr. Soc.* **69**, 607–621.

Bonilla, M. G., Mark, R. K. & Lienkaemper, J. J. 1984. Statistical relations among earthquake magnitude, surface rupture length and surface fault displacement. *Bull. Seism. Soc. Am.* **74**, 2379–2411.

Crone, A. J. & Haller, K. M. 1991. Segmentation and the coseismic behaviour of basin and range normal faults: Examples from east-central Idaho and southwestern Montana, U.S.A. *J. Struct. Geol.* **13**, 151–164.

Dart, C., Collier, R. E. Ll., Gawthorpe, R., Keller, J. V. A. & Nichols, G. 1994. Sequence stratigraphy of (?) Pliocene–Quaternary synrift, Gilbert-type fan deltas, northern Peloponnesos, Greece. *Mar. Pet. Geol.* **11**, 545–560.

Destro, N. 1995. Release fault: A variety of cross fault in linked extensional systems, in the Sergipe–Alagoas Basin, NE Brazil. *J. Struct. Geol.* **17**, 615–630.

Doutsos, T. & Poulimenos, G. 1992. The geometry and kinematics of active faults and their seismotectonic significance in the western Corinth–Patras Rift (Greece). *J. Struct. Geol.* **14**, 689–700.

Ferentinos, G., Papatheodorou, G. & Collins, M. B. 1988. Sediment transport processes on an active submarine fault escarpment: Gulf of Corinth, Greece. *Mar. Geol.* **83**, 43–61.

Gawthorpe, R. G. & Hurst, J. M. 1993. Transfer zones in extensional basins: their structural style and influence on drainage development and stratigraphy. *J. Geol. Soc. Lond.* **150**, 1137–1152.

Gawthorpe, R. G., Fraser, A. J. & Collier, R. E. Ll. 1994. Sequence stratigraphy in active extensional basins: implications for the interpretation of ancient basin fills. *Mar. Pet. Geol.* **11**, 642–658.

Hanks, T. C. & Kanamori, H. 1979. A moment magnitude scale. *J. Geophys. Res.* **84**, B5, 2348–2350.

Heezen, B. C., Ewing, M. & Leonard Johnson, G. 1966. The Gulf of Corinth floor. *Deep-Sea Res.* **13**, 381–411.

Higgs, B. 1988. Syn-sedimentary structural controls on basin deformation in the Gulf of Corinth, Greece. *Basin Res.* **1**, 155–165.

IGME 1970. Nemea 1:50 000 Geological Sheet, Athens, Greece.

IGME 1971. Erithres 1:50 000 Geological Sheet, Athens, Greece.

IGME 1982. Kandhila 1:50 000 Geological Sheet, Athens, Greece.

IGME 1984a. Kaparellion 1:50 000 Geological Sheet, Athens, Greece.

IGME 1984b. Megara 1:50 000 Geological Sheet, Athens, Greece.

IGME 1984c. Perachora 1:50 000 Geological Sheet, Athens, Greece.

IGME 1985. Sofikon 1:50 000 Geological Sheet, Athens, Greece.

IGME 1989a. Seismotectonic map of Greece 1:500 000, Athens, Greece.

IGME 1989b. Xilokastron 1:50 000 Geological Sheet, Athens, Greece.

IGME 1993. Dervenion 1:50 000 Geological Sheet, Athens, Greece.

Jackson, J. A. 1994. Active tectonics of the Aegean Region. *A. Rev. Earth Planet. Sci.* **22**, 239–271.

Ma, X. Q. & Kusznir, N. J. 1995. Coseismic and postseismic subsurface displacements and strains for a dip-slip normal fault in a three-layer elastic gravitational medium. *J. Geophys. Res.* **100**, **No. B7**, 12813–12828.

Mercier, J-L., Delibassis, N., Gauthier, A., Jarrige, J., Lemeille, F., Philip, H., Sebrier, M. & Sorel, D. 1979. Le neotectonique de l'Arc Egeen. *Revue Geogr. phys. Geol. dyn.* **21**, 67–92.

Myrianthis, M. L. 1982. Geophysical study of the epicentral area of the Alkyonides Islands Earthquakes, central Greece. Geophysical Institute of Hungary. *Geophys. Trans.* **28/2**, 5–17.

Pavlides, S. B. & Mountrakis, D. M. 1987. Extensional tectonics of northwestern Macedonia, Greece, since the late Miocene. *J. Struct. Geol.* **9**, 385–392.

Perissoratis, C., Mitropoulos, D. & Angelopolous, I. 1986. Marine geological research at the eastern Corinthiakos Gulf. *IGME Geol. Geophys. Res.* Athens, Special Issue, 381–401.

Piper, D. J. W., Stamatopoulos, L., Poulimenos, G., Doutsos, T. & Kontopoulos, N. 1990. Quaternary history of the Gulfs of Patras and Corinth, Greece. *Zeitschrift fur Geomorphologie N. F.* **34**, **4**, 451–458.

Poulimenos, G., Gisbert, A. & Doutsos, T. 1989. Neotectonic evolution of the central section of the Corinth Graben. *Z. dt. geol. Ges.* **140**, 173–182.

Poulimenos, G. 1993. Tectonics and sedimentation in the western Corinth graben, Greece. *Neues. Jb. Geol. Palaont. Mh.* **H10**, 607–630.

Roberts, G. P. & Gawthorpe, R. L. 1995. Strike variation in deformation and diagenesis along segmented normal faults: an example from the Gulf of Corinth. In: *Hydrocarbon habitat in rift basins* (edited by Lambiase, J.). *Spec. Publ. Geol. Soc. Lond.* **80**, 57–74.

Roberts, G. P. & Koukouvelas, I. In press. Structural and seismological segmentation of the Gulf of Corinth Fault System: implications for models of fault growth. *Annali di Geofisica.*

Roberts, S. & Jackson, J. A. 1991. Active normal faulting in central Greece: An overview. In: *The Geometry of Normal Faults* (edited by Roberts, A. M., Yielding, G. & Freeman, B.). *Spec. Publ. geol. Soc. Lond.* **56**, 125–142.

Schwartz, D. P. 1989. Paleoseismicity, persistence of segments, and temporal clustering of large earthquakes—examples from the San Andreas, Wasatch, and Lost River fault zones. In: Proceedings of Conference XLV—*Fault Segmentation and Controls of Rupture Initiation and Termination* (edited by Schwartz, D. P. & Sibson, R. H.). U.S. geol. Surv. Open-file Rep. **89–315**, 361–375.

Slemmons, D. B. 1977. Faults and earthquake magnitude. *U.S. Army Corp. of Engrs, Waterways Exp. Sta. Misc. Pap.* **S-73-2**.

Taymaz, T., Jackson, J. A. & McKenzie, D. P. 1991. Active tectonics of the north and central Aegean. *Geophys. J. Int.* **106**, 433–490.

Wu, D. & Bruhn, R. L. 1994. Geometry and kinematics of active normal faults, South Quirrh Mountains, Utah: implication for fault growth. *J. Struct. Geol.* **16**, 1061–1076.

Wyss, M. 1979. Estimating maximum expectable magnitude of earthquakes from fault dimensions. *Geology* **7**, 336–340.

Zhang, P., Slemmons, D. B. & Mao, F. 1991. Geometric pattern, rupture termination and fault segmentation of the Dixie Valley–Pleasant Valley active normal fault system, Nevada, USA. *J. Struct. Geol.* **13**, 165–176.